CLM-P589

UKAEA

Preprint

DITE TOKAMAK PRESENTATIONS

NINTH EUROPEAN CONFERENCE ON CONTROLLED FUSION AND PLAMA PHYSICS OXFORD 17 - 21 SEPTEMBER 1979

CULHAM LABORATORY
Abingdon Oxfordshire

1979

DITE TOKAMAK PRESENTATIONS

NINTH EUROPEAN CONFERENCE ON CONTROLLED

FUSION AND PLASMA PHYSICS

OXFORD 17 - 21 SEPTEMBER 1979

DITE TOKAMAK PRESENTATIONS

Papers submitted to the Ninth Conference on Controlled Fusion and Plasma Physics

Oxford September 1979

- - - - - - - - - - -

There will also be an invited review paper by Dr J.W.M. Paul which will be reproduced in a separate pre-print.

Culham Laboratory

August 1979

KS

LOW-Q DISCHARGES IN DITE TOKAMAK

J. Hugill, A.J. Wootton, K.B. Axon, B.A. Powell, R. Prentice, D.D.R. Summers and C.M. Wilson

Culham Laboratory, Abingdon, Oxon, OX14 3DB, UK
(Euratom/UKAEA Fusion Association)

ABSTRACT Reproducible, grossly stable discharges with $2.4 > q_L > 2.2$ for up to 100 ms are produced in DITE tokamak by careful attention to operating procedures. The m.h.d. behaviour is described and an energy balance given. The confinement properties are not inferior to those at higher toroidal field.

- - - - - - - - - - - -

The main parameters of the DITE Tokamak during these experiments are $R = 1.17$ m, $a_L = 0.26$ m, $B_T = 1.35$ T, $I = 160 - 175$ kA, giving $q_L = 2.2 - 2.5$. Two limiters, each consisting of two semi-circular arcs, spaced at least 30 mm from the vacuum vessel, are of either Mo or Ti. The bundle divertor is not used. Feedback control keeps the plasma centre at $R = 1.16$-1.17 m. The eight box-shaped sections of the vacuum vessel are connected toroidally by bellows and copper straps and have a time constant for vertical field penetration of ~ 4 ms. The torus is gettered with titanium for one hour before operation and between discharges (10 mins) using between one and three Varian Ti balls spaced around the vacuum vessel. Cold gas feed via piezoelectric valves maintains or increases the density during a discharge.

The discharge current is first raised to ~ 100 kA ($q_L = 4$) in 3 ms and is then ramped more slowly to 160 - 175 kA in 40 - 50 ms, either immediately or after a 100 ms plateau at the lower current level. The gas feed rate is usually held constant during the second current ramp, at a low level giving constant $\bar{n}_e \sim 10^{19}$ m^{-3}, or sufficient to increase $\bar{n}_e$ at a rate up to about 3×10^{20} m^{-3} s^{-1}. The general behaviour of the discharge does not seem to depend critically on the gas feed rate. Fig. 1 shows the various paths followed in I v n space. The highest density was reached with a 50 ms 0.3 MW pulse of neutral beam injection at 22 kV.

Operation at low q in DITE depends mainly on the following conditions

a) Cleanliness of the vacuum wall, provided in this case by gettering.

b) Absence of mhd modes with m = 2, measured by coils outside the plasma column.

c) Removal of heavy metals from the vacuum system. Although low-q operation is possible with Mo limiters, it is much easier with limiters of Ti.

d) Conditioning of the vacuum vessel and/or limiters and the patience

of the experimentalist. The first discharges usually disrupt even at high q but the behaviour gradually improves. Violent disruptions can themselves cause deconditioning and affect the subsequent discharge but in a well conditioned vacuum vessel the discharge recovers from minor disruptions even during the low-q plateau.

Sixteen coils positioned at r = 0.29 m around the minor aximuth measure the amplitude and poloidal mode number of magnetic fluctuations in B_p. Soft X-ray diodes are used to detect sawtooth oscillations and measure the radius of phase inversion. Sawtooth oscillations are also seen on the 2 mm microwave interferometer.

Figure 2 shows the time behaviour of the main discharge parameters and the mhd behaviour, for a low-q D_2 discharge with Ti limiters. As the current passes through the levels where $3.1 > q_L > 2.7$ a rapidly growing m = 3 mode is seen associated with a small + ve spike on the loop voltage. Because of its rapid growth rate and its persistence to $q_L < 3$, this is thought to be a kink mode. At the same time a more slowly growing m = 2 mode is seen which may persist at low-q and, in a badly conditioned vacuum vessel, leads to disruption. This is probably a tearing mode centred at the q = 2 surface. During the low-q current plateau, strong sawtooth oscillations are seen with a period of 2.5 ms. The radius of the q = 1 surface obtained from the T_e profile is 0.14 m, with or without neoclassical corrections to the resistivity. After Abel inversion, the profiles of sawtooth oscillations in soft X-ray signals and in the line of sight density show that the inversion point lies between r = 0.11 m and r = 0.13 m. The amplitude of the density fluctuations at r = 0 is $\sim$ 5%.

Figure 3 gives the profiles of T_e, n_e, T_i and total radiation for the discharge shown in Fig. 2. The profiles of T_i were made with a neutral particle analyser scanned across the minor radius, observing at an angle of 7.5° to the major radius. All the profiles are quite flat inside the q = 1 surface. With neoclassical corrections, there is no resistance anomaly, indicating low impurity content. Total radiation, including charge-exchange neutrals, accounts for only (32^{+16}_{-5}) of the ohmic input. The main impurity is probably Ti from the walls and limiters. Table I lists the parameters derived from these profiles and an energy balance at r = 0.2 m is given in Fig. 4.

Comparison with discharges at similar current and density at higher q, shows that the confinement properties of the low-q discharge are similar

to those at higher B_T, the profiles being somewhat broader and T_{eo} and n_{eo} lower.

Preliminary attempts to raise the current rapidly to achieve $q_L < 2$ were unsuccessful. A major disruption occurs, preceded by very rapidly growing mhd modes with undetermined mode number. A more systematic attempt to reach $q_L < 2$ will be made in due course. The effect of using the DITE bundle divertor will also be studied.

ACKNOWLEDGEMENTS

We are indebted to Mr G.W. Reid and the DITE operating team and to Dr J.W.M. Paul for supporting this work. Drs J.A. Wesson and F. Alladio provided computations of mhd stability, with the assistance of Mrs M. Turner. Mr J.B.B. Percival provided the data from the neutral particle analyser.

REFERENCES

(1) S.J. Fielding et al, Nuclear Fusion 17 (1977) 1382.

(2) J.A. Wesson, Nuclear Fusion 18 (1978) 87.

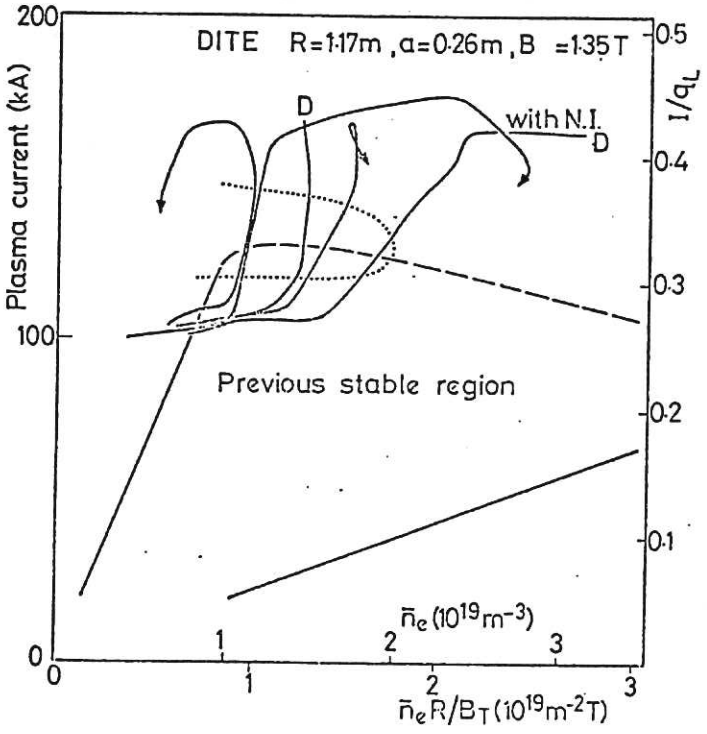

Fig. 1. Trajectory of various discharges in I v $\bar{n}_e$ space. Region of stable operation obtained previously (1) is shown. Dotted curve encloses area where enhanced m = 3 (kink) activity is observed.

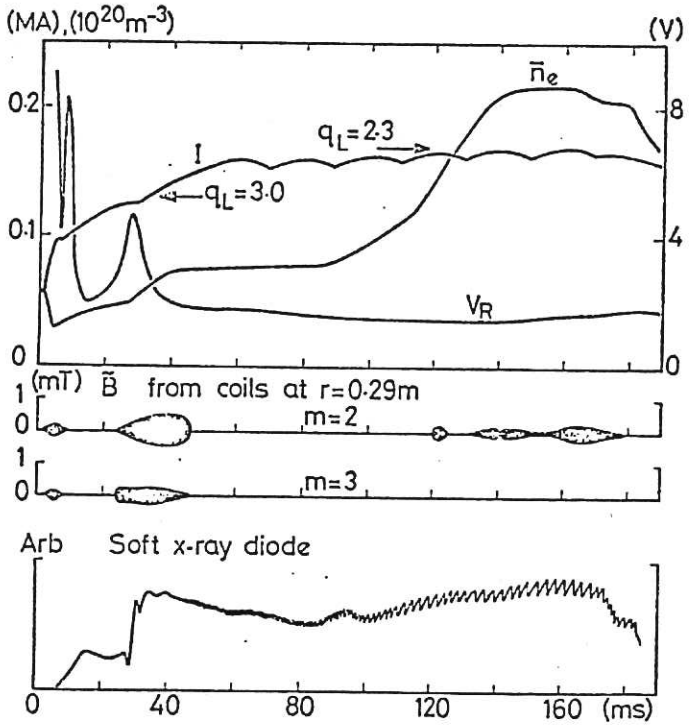

Fig. 2. Time behaviour of various parameters in a low-q discharge in deuterium.

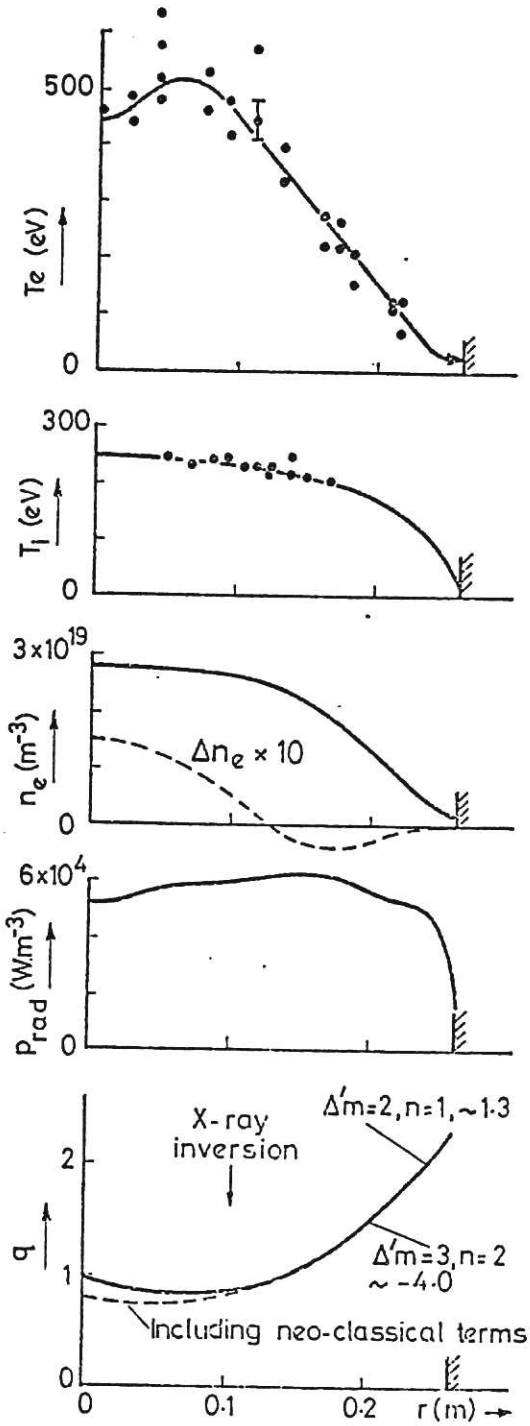

Fig. 3. Radial profiles of various parameters at t = 150 ms. The q profile shown is derived from the electron temperature, including neoclassical terms. Marked is the X-ray sawtooth oscillation inversion point, and the parameter Δ' from a tearing mode calculation (2).

Fig. 4. The energy balance inside r = 0.2 m at t = 150 ms.

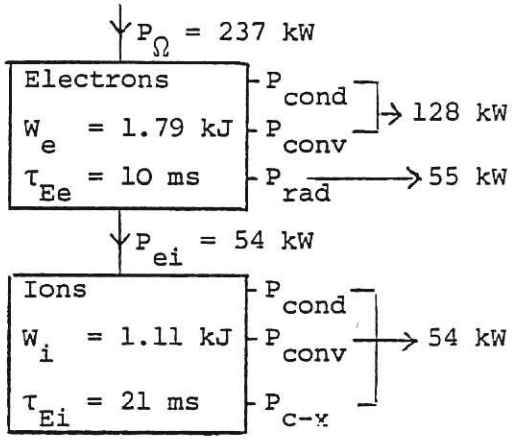

Table I - Main discharge parameters

R	= 1.17 m	N	= 3.4 x 10^{18} m^{-1}
a	= 0.26 m	$\langle T_e \rangle$	= 312 eV
B_T	= 1.35 T	$\langle T_i \rangle$	= 239 eV
I	= 170 kA	Z_{eff}	from resistance
V_R	= 1.5 V	a) $j \sim T_e^{3/2}$	1.4
q_L	= 2.3	b) N-C corrections	1.0
τ_E	= 12 ms	$\nu^*_{e(min)}$	= 0.6 at r = 0.1 m
β_p	= 0.20	ν^*_i	= 0.8 at r = 0.2 m
P_{rad}/P_{OH}	= 0.32		

NEUTRAL INJECTION HEATING IN DITE

R.D. Gill, K.B. Axon, G.A. Baxter, W.H.M. Clark, R.S. Hemsworth, J. Hugill, J.W.M. Paul, J.B.B. Percival, R. Prentice, B.A. Powell and A.A. Mirin*

Culham Laboratory, Abingdon, Oxon, OX14 3DB, UK
(Euratom/UKAEA Fusion Association)

*Lawrence Livermore Laboratory, U.S.A.

We have recently operated DITE tokamak[1] (R = 117 cm, a = 26 cm, $B_\phi \leq 2.8$ T) with the 1.2 MW, 50 ms, 30 keV hydrogen neutral injection system[2]. Four injectors with McKenzie bucket design are fitted to two tangential beam lines directed with the plasma current (co-injection). The measured ion species extracted from the sources are $I(H^+):I(H_2^+):I(H_3^+)$ = 77:18:5. The tokamak plasma was H^+.

The main experiments were carried out with molybdenum limiters and titanium gettered torus walls. Typical parameters with and without injection are shown in the table. The considerable drop in loop volts (V_ℓ) with no electron temperature change is suggestive of the presence of a beam driven Ohkawa current although this is difficult to prove. Standard diagnostics were used to measure most of the main plasma parameters and a mass selective neutral particle analyser measured the ion temperature (T_i) profiles. The ion temperature increases linearly with neutral injection power per unit particle ($P/\bar{n}_e$) at first (Fig. 1) but saturates at a value approaching 900 eV. The electron temperature (T_e) did not rise but there was usually a considerable rise in electron density (n_e) during injection. One feature of our experiment which is not well illustrated by this data was the observation on many discharges of plasma disruptions when injecting more than 600 kW.

We have used these injection results to determine values for the ion thermal conductivity (K_i) in the absence of disruption. The energy balance equation for the ions at minor radius r can be written[3] in the steady state as

$$-\frac{1}{r}\frac{\partial(rQ_i)}{\partial r} + n_i e v E_r + Q_{ei} + Q_{NI} + \frac{3}{2} n_e n_o \langle\sigma v\rangle_i T_o - \frac{3}{2} n_i n_o \langle\sigma v\rangle_x (T_i - T_o) = 0$$

where the radial heat flux (Q_i) and the radial velocity (v) are determined by

$$-\frac{1}{r}\frac{\partial}{\partial r}(r\, n_i\, v) + n_e n_o \langle\sigma v\rangle_i = 0$$

$$Q_i = -K_i n_i \frac{\partial T_i}{\partial r} + y\, n_i\, T_i\, v$$

where n_o and T_o are the neutral density and temperature. Q_{ei} and Q_{NI} are the heat input terms due to electron-ion collisions and neutral injection

and are calculated in the standard way[4]. The terms involving $\langle \sigma v \rangle_i$ and $\langle \sigma v \rangle_x$ are the source terms due to ionisation and charge-exchange of neutrals in the plasma. y is a coefficient which is approximately 2.5 for DITE and we have assumed that the radial electric field $E_r = 0$, although our values of K_i are insensitive to this assumption.

In order to solve these equations for K_i we must know n_o and T_o. The former was determined from the intensity of the neutral particle analyser signals and the latter by assuming $T_o(r) = T_i(r + \lambda/2)$ where λ is the neutrals mean free path. This assumption is justified because the strong inward gradient of n_o in a tokamak plasma implies that neutrals at r have originated, on average, at $(r + \lambda/2)$. The ion heat fluxes determined by this procedure are shown in Fig. 2 and the values of K_i deduced are shown in Fig. 3 as a function of radius. The theoretical neoclassical[5] values are also shown and are less than the experimental values by a factor of about 5 both with and without neutral injection. The other main result of these calculations was to show that at the highest ion temperatures the heat loss to the cooler electrons was a dominant process and that this caused the observed saturation in T_i as a function of injection power. The plot of $\nu = qR/v_i\tau_i$ as a function of radius (Fig. 4) shows that the ions are in the plateau region during ohmic heating but move into the banana regime during strong neutral injection heating.

We have also compared our results with the predictions of a Fokker-Planck/transport code developed by Mirin et al[6]. The code uses empirical values for the transport coefficients, the Hughes-Post method for treating neutrals and a two regime Fokker-Planck method for determining the heating effects of the neutral injection. Specifically we assume that $K_e = 5 \times 10^{17}/n_e$ cm^2 s^{-1}, $K_i = 10^4$ cm^2 s^{-1} and $D(r) = [10^3 + 9 \times 10^3 (r/a)^2]$ cm^2 s^{-1}, since these values give good agreement with our discharges without neutral injection. The code was used to compute the results shown in Fig. 1 and agreement with experiment is good except at the highest power levels. This difference appears because the code does not correctly model the impurity radiation losses and hence predicts substantial electron heating which is not observed experimentally.

We have also carried out an overall electron energy balance (Fig. 5) both with and without 1.0 MW of neutral injection. The radiated power determined from a radially scanned thermopile showed a very striking increase on injection, but the energy lost due to conduction and convention remained approximately constant. The large radiation losses implies the presence of

high Z atoms in the discharge (probably Mo) and for this reason it was decided to change the fixed limiters to titanium together with a pair of adjustable carbon limiters.

Preliminary experiments with no Mo in the torus showed a dramatic reduction in the total radiated power by a factor of ~ 5 and electron heating was observed during injection into higher density discharges. The occurrence of disruptions was very much reduced and with injection of ~ 1.0 MW of H into a D^+ plasma it was possible to reach peak plasma $\hat{\beta}_T = 1.5\%$ and $\beta_\theta = 0.65$. It was also found that the ion temperature increased linearly with $(P/\bar{n}_e)$ up to P = 1.0 MW.

REFERENCES

(1) PAUL, J.W.M. et al, Proc. 6th Int. Conf. on Plasma Physics and Contr. Nuclear Fusion, Berchtesgaden 1976, (IAEA Vienna 1977) 2, 269.
(2) HEMSWORTH, R.S. et al, Joint Varenna-Grenoble Int. Symp. on Heating in Toroidal Plasmas, Grenoble, 3-7 July 1978.
(3) HINTON, F.L., et al, Phys. Rev. Lett. 29 (1972) 698.
(4) AXON, K.B. et al, Nuclear Fusion 18 (1978) 981.
(5) Equipe TFR, Proc. 8th Europ. Conf. on Controlled Fusion and Plasma Phys. 2 (Prague 1977) 1.
(6) MIRIN, A.A. et al, J. Comput. Phys. 23 (1977) 23.

Injection		off	on		off	on
B_ϕ	(T)	2.0	2.0	q(limiter)	4.04	4.04
I_G	(kA)	150	150	q(centre)	1.54	2.18
V_ℓ	(v)	3.01	1.95	$\bar{n}_e$ (cm^{-3})	1.2×10^{13}	1.6×10^{13}
Z_e		4.92	3.19	$\hat{T}_e$ (eV)	520	520
P_Ω	(kW)	451	290	T_i (eV)	290	900
P	(kW)	0	800			

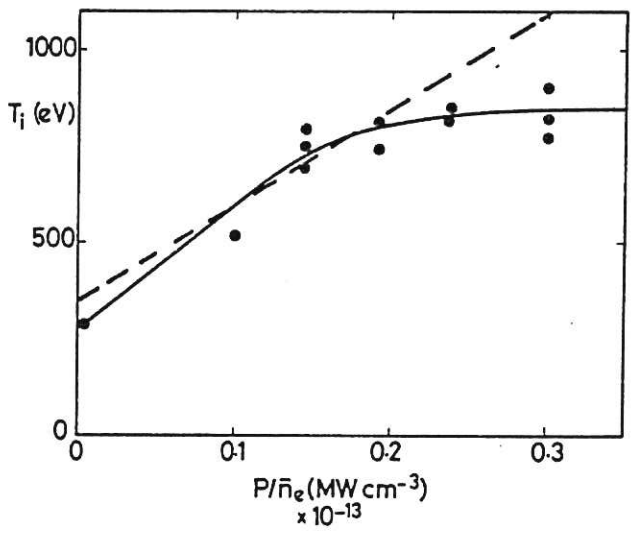

Fig. 1 Ion temperature as a function of $P/\bar{n}_e$. The broken line shows the transport calculation.

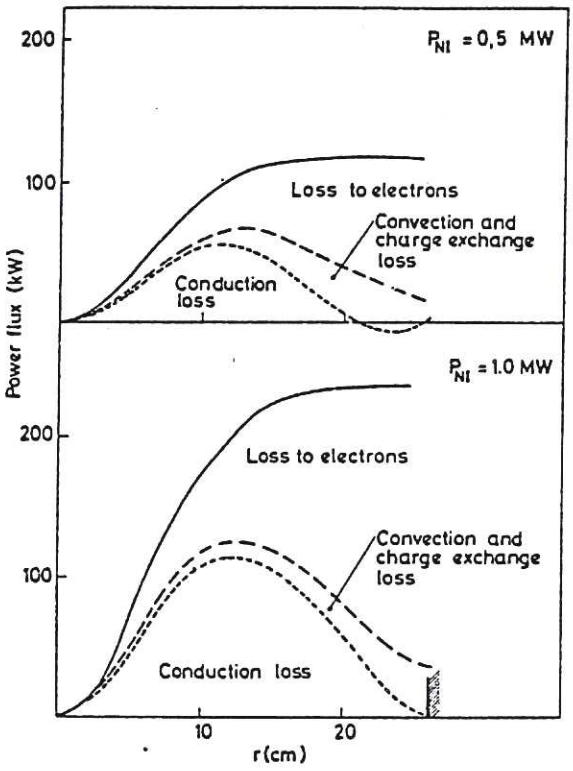

Fig. 2 Total power flux integrated over a toroidal surface as a function of minor radius.

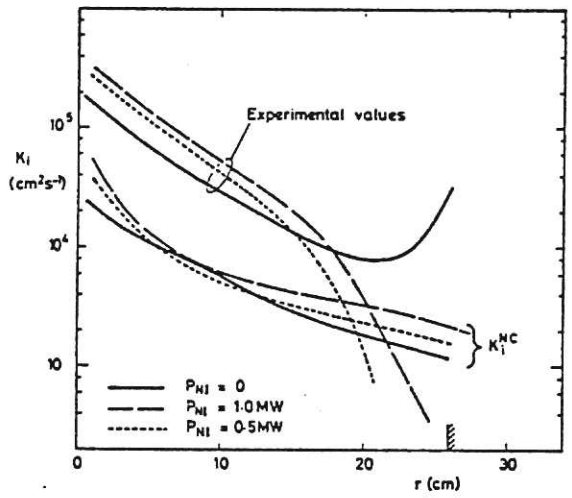

Fig. 3 Experimental and theoretical ion thermal conductivity as a function of minor radius.

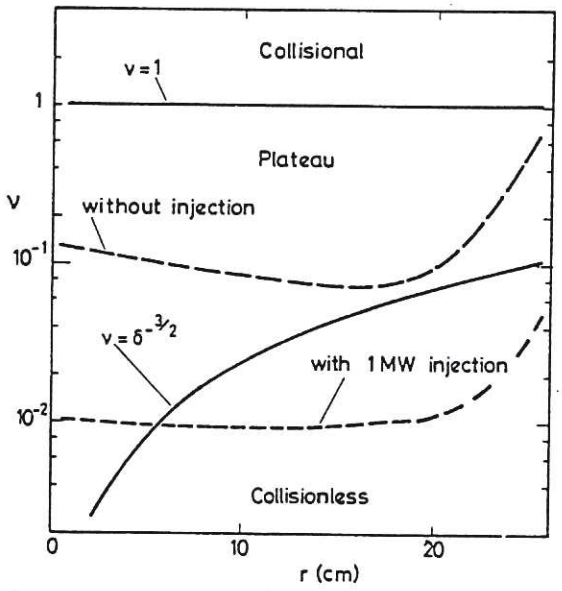

Fig. 4 The collisionality parameter ν as a function of minor radius. The injection takes the plasma from the plateau to the collisionless regime.

Electron energy balance

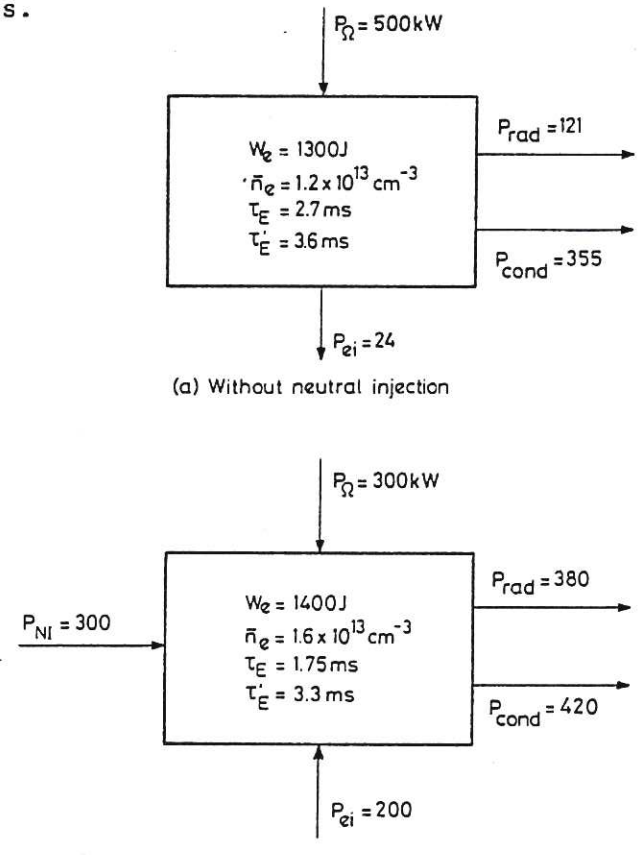

Fig. 5 Electron heat balance (a) without and (b) with neutral injection.

RESULTS FROM THE DITE BUNDLE DIVERTOR

S.J. Fielding, J.W.M. Paul and A.J. Wootton
Culham Laboratory, Abingdon, Oxon, OX14 3DB, UK
(Euratom/UKAEA Fusion Association)

ABSTRACT

The DITE bundle divertor has been operated in conjunction with a titanium gettered torus wall and results compared with those without gettering. Higher densities have been achieved with gettering and diversion. Preliminary observations with injection and diversion are reported.

INTRODUCTION

Both the bundle divertor[1] and gettering of the torus wall[2] have been used, previously separately and now together, to reduce impurities in DITE. The bundle divertor acts by producing a separatrix, outside of which a scrape-off layer exists. Particles and energy are exhausted via this layer onto a target in a chamber outside the main torus, thus reducing the plasma-wall interaction. Impurities produced at the wall are ionised and removed to the target. Typically, low Z impurities are reduced to ~ 0.25 and high Z impurities to $\lesssim 0.1$, of their previous concentrations in the main discharge.

Gettering operates by chemically trapping particles on the wall. This reduces the low Z impurities to ~ 0.12 of their previous values. Because the working gas is trapped, additional gas feed is required to maintain the density. The high Z impurities concentration is reduced to ~ 0.2 at high densities.

LOW DENSITIES

Preliminary results with and without the divertor, for both non-gettered and gettered walls, are compared in Figs. 1 and 2. The divertor is switched on in the middle of the tokamak pulse for a duration of about 150 ms. Other parameters are $R_p = 1.17$ m, $a_{lim} \sim 0.26$ m, $a_{sep} \sim 0.16 - 0.19$ m, $B_{To} \sim 0.9$ T, $I_p \sim 50$ kA, $q_{lim} \sim 5.2$, $q_{sep} \sim 2.0 - 2.8$, $T_{eo} \sim 300$ eV. The limiter material is Mo. The gettering, between each discharge, covers about 50% of the torus walls with two monolayers of Ti. The data presented here is derived from a few short periods of operation and is not always consistent.

In a non-gettered torus, operation of the divertor increases the plasma current and decreases the volts. The opposite effect occurs in a gettered torus, where the decrease in current may be caused by the expulsion of a component of runaway electrons. The effect does not occur when low initial density is avoided.

After the initial gas filling there is a steady gas feed during the

discharge. In a non-gettered torus, diversion reduces the steady density to 0.35 of its initial value. In a gettered torus there is a smaller reduction to 0.7, although a steady state is difficult to obtain. With ungettered walls, refueling is mainly from the walls with the gas feed constituting a small component of the total hydrogen flux into the plasma. Diversion approximately halves the flux of ions to the wall thereby reducing the recycling and hence the density. With gettered walls this wall recycling is reduced before diversion and the gas feed is increased to compensate. The hydrogen flux into the plasma is now dominated by the gas feed, which is not greatly affected by the divertor because at these densities the screening efficiency for hydrogen is low (< 0.2). This explains the lower density drop with gettered walls.

The intensity of the O II (4414 Å) line is assumed to represent the influx of oxygen at the edge. Operation of the divertor reduces this influx less in a gettered than in an ungettered torus (Table I) probably because of a smaller change in the particle flux to the wall. The intensities of the O VI (1031 Å) and O VII (1623 Å) lines, which arise inside the separatrix, are assumed to represent the influx of oxygen inside the separatrix. The decrease in these lines on diversion (Figs. 1 and 2; Table I) results from both the decreased source at the wall and the screening effect. Thus the screening efficiency (ξ_{SO}) can be calculated (Table I). For both lines gettering reduces the intensities to 0.12.

The total radiated power from $r < 0.1$ m drops dramatically when the divertor is switched on with an ungettered torus, but hardly changes with a gettered torus (Figs. 1 and 2; Table IIa). However, it changes during the pulse even without diversion (Table IIb) so that the effect should be measured by the ratio divertor on to off at the same time (Table IIc). The total radiation before diversion with gettering is about half that without gettering and so the absolute value after diversion is about the same in both cases.

The measured X-ray anomaly factors (ζ), (Table III) demonstrate the reduction of heavy metals and the production of pure plasma ($\zeta \sim 1$). An understanding of the behaviour of the radiated power and X-ray anomaly factor requires clearly consistent sets of data including profiles of both and the impurity species.

HIGH DENSITY OPERATION

In preliminary experiments, gettering without diversion did not extend the operating range of density, but when combined with diversion the range was extended by a factor of about two (Fig. 3). Diverted discharges recover

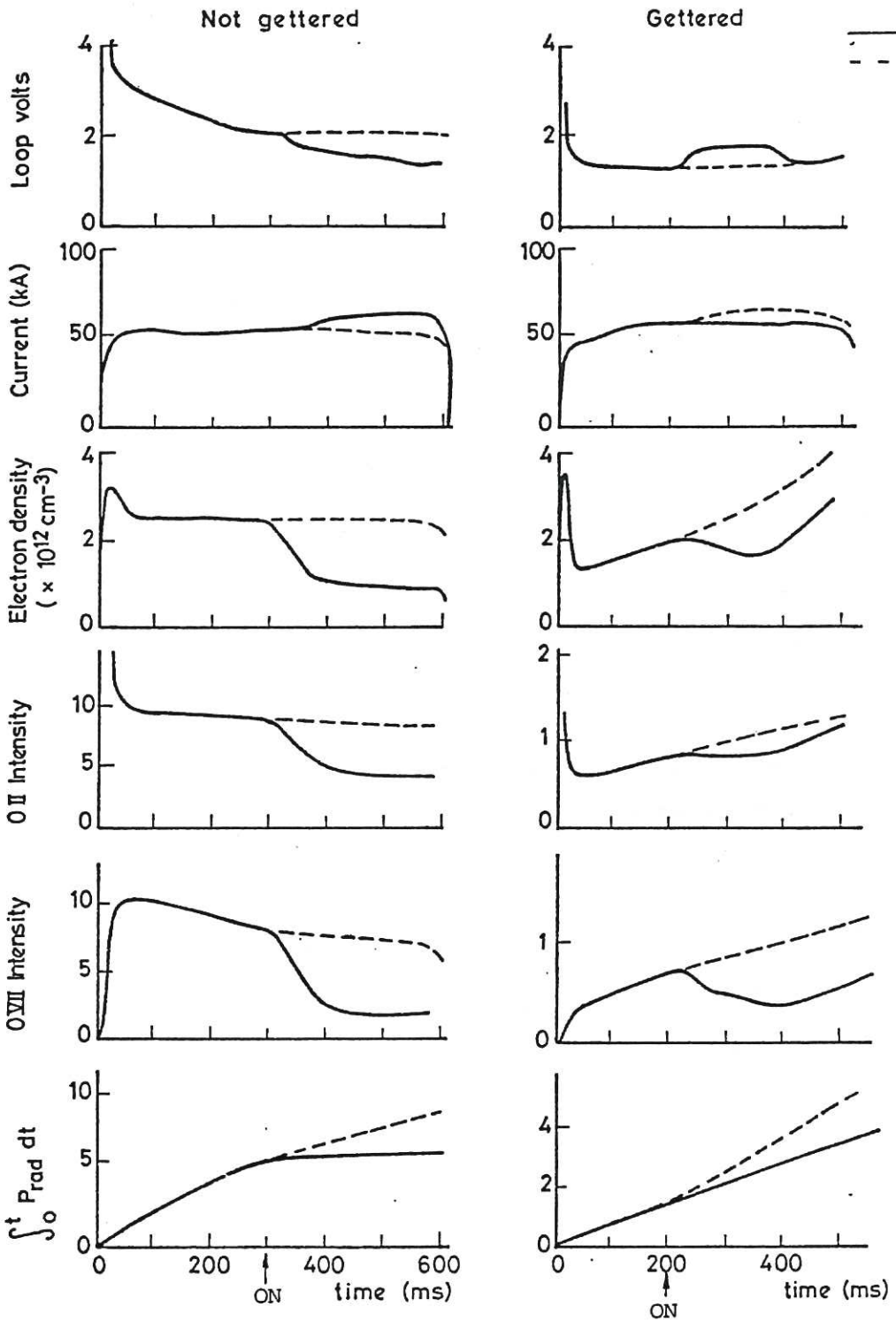

Fig. 1

Fig. 2.

TABLE I: Normalised Intensities of Oxygen Lines

	Divertor off		Divertor on		ξ_{SO}
	O II	O VII	O II	O VII	
Ungettered	1	1	0.5	0.25	50%
Gettered	0.12	0.13	0.1	0.05	46%

more readily from soft disruptions during gas feed probably because of the weaker interaction with the wall. More perseverance might also allow higher density operation with gettering alone. Parameters have been increased to $n_{eo} \sim 6 \times 10^{19}$ m^{-3}, $\bar{n}_e \sim 2 \times 10^{19}$ m^{-3}, $\tau_E \sim 11$ ms, $\beta_p \sim 0.75$ and $\langle \beta_T \rangle$ inside the separatrix $\lesssim 0.3\%$.

INJECTION AND DIVERSION

Preliminary experiments with the divertor and 0.2 MW (100 ms) of injection power into an ungettered torus have shown beam trapping of up to 50 %. The density increase on injection corresponds roughly with the trapped beam and is unaffected by diversion. There is a large influx of impurities (O, C, Fe) resulting from the absorbed and not the transmitted power. The divertor is not as effective at controlling the beam induced impurities and radiative loss as it is for the comparable ohmic power input. The beam appears to be lost by charge-exchange, because of the low density, and by orbit effects, because of the low current. These effects will be reduced in the near future by operating at higher density and current (lower q) and after that by a new full field divertor.

ACKNOWLEDGEMENTS

We thank Drs J. Hugill, P.E. Stott and P.J. Lomas and Messrs K.B. Axon, B.A. Powell and R. Prentice for advice and assistance and the DITE operation team.

REFERENCES

(1) S.J. Fielding et al, Proc. 8th Europ. Conf. on Controlled Fusion and Plasma Physics, Prague (1977) 1, 36.
(2) S.J. Fielding et al, Nuclear Fusion 17 (1977) 1383.
(3) J.W.M. Paul et al, Proc. 8th Europ. Conf. on Controlled Fusion and Plasma Physics, Prague (1977) 2, 49.

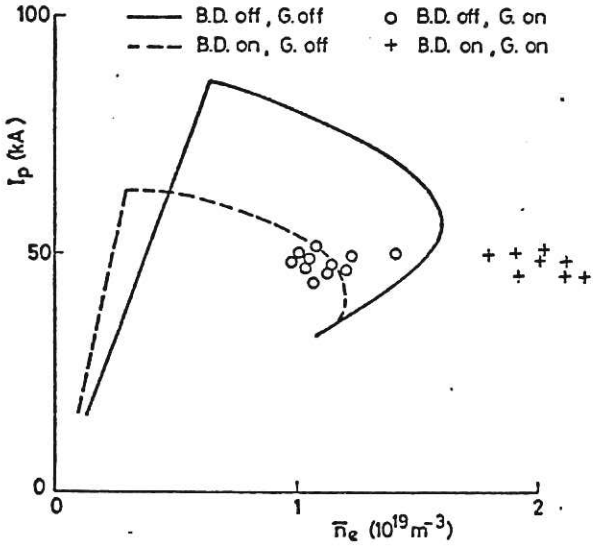

Fig. 3.

TABLE II: Ratios of radiated power

	After/Before BD on (a)	BD off (b)	On/off same t (c)
Ungettered	0.19	0.67	0.28
Gettered	1.0	1.5	0.67

TABLE III: X-ray Anomaly Factors

Divertor	Ungettered[3]	Gettered
Off	400	4.2
On	80	1.0

POLARIZATION AND MILLISECOND SPECTRAL MEASUREMENTS OF ELECTRON CYCLOTRON EMISSION FROM DITE TOKAMAK

D.J. Campbell[+], W.H.M. Clark, A.E. Costley[*], P.J. Fielding, L.C. Robinson[+], G.D. Tait[‡] and B. Walker[*]

Culham Laboratory, Abingdon, Oxon, OX14 3DB, UK
(Euratom/UKAEA Fusion Association)

+ University of Sydney, Sydney, Australia
* Division of Electrical Science, National Physical Laboratory, Teddington, U.K.
‡ University of Maryland, College Park, Maryland U.S.A.

ABSTRACT

Measurements of electron cyclotron emission (ECE) spectra from DITE tokamak on a millisecond timescale are reported along with the corresponding electron temperature profiles. Preliminary measurements of the Stokes parameters for the polarization of the emission at the second harmonic are also reported. A theoretical expression for the angular variation of the optical depth of each mode of polarization of the second harmonic in a finite density plasma is used to qualitatively explain the low degree of polarization observed.

MILLISECOND MEASUREMENTS

The measurement of ECE spectra from tokamak discharges using fourier-transform spectroscopy is becoming a routine diagnostic[1,2]. If the emission is due to thermal electrons the radial electron temperature profile may be determined from the line profile of an optically thick harmonic[3]. On the DITE tokamak a vibrating mirror interferometer, with a scanning time of 14 ms, is used for this purpose. Repetitive measurements in shorter timescales have proved difficult[4]. Here we report spectral measurements taken with a novel Michelson interferometer, where the scanning device is a rotating mirror providing a scanning time of 1 ms and repetition rate of 100 Hz. In Fig. 1 the spectra measured by both instruments for similar steady state discharges show good agreement, (magnetic field = 2 T, mean density = 4.5 x 10^{13} cm^{-3} and peak electron temperature from Thomson scattering = 700 eV). Figure 2 shows a sequence of electron temperature profiles determined from spectra measured (from several shots) in the early transient phase of the DITE discharge. The plasma is assumed to be optically thick in the central region, (field = 2 T, density = 1 x 10^{13} cm^{-3}, temperature = 1 keV). Interference prevented measurements from being made during the first 10 ms. The same detector (a hot electron bolometer) is used for both instruments but is not yet calibrated accurately. This may account for the apparent asymmetry

in the profiles.

POLARIZATION MEASUREMENTS

Previous measurements have not completely determined the polarization of the ECE[5,6]. If the x and y components of the electric field vector of a monochromatic wave propagating in the z-direction are given by

$$E_x = E_{xo} \cos(\omega t - kz + \delta_x) \qquad E_y = E_{yo} \cos(\omega t - kz + \delta_y)$$

then the polarization may be completely defined by the four Stokes parameters:

$$I = E_{xo}^2 + E_{yo}^2 \qquad M = E_{xo}^2 - E_{yo}^2$$

$$C = 2E_{xo} E_{yo} \cos(\delta_x - \delta_y) \qquad S = 2E_{xo} E_{yo} \sin(\delta_x - \delta_y)$$

where for a monochromatic wave: $I - \sqrt{M^2 + C^2 + S^2} = 0$. For a beam composed of an incoherent ensemble of waves in a narrow spectral bandwidth the totals of the Stokes parameters are such that

$$I_t - \sqrt{M_t^2 + C_t^2 + S_t^2} = I_t - I_p = I_o.$$

Thus the beam intensity is composed of a polarized component I_p and an unpolarized component I_o such that the degree of polarization

$$p = \frac{I_p}{I_o + I_p}.$$

With a fixed frequency (112 GHz) polarimeter consisting of a Fabry-Perot interferometer (bandwidth 3 GHz), rotating polarizer and a quarter-wave plate, we have determined the Stokes parameters for radiation at the second harmonic from the centre of a discharge under conditions similar to those of Fig. 2, viz:

$$I = 4.5 \pm 1.5 \qquad M = 4 \pm 1 \qquad C = 0 \pm 1.5 \qquad S = -1.0 \pm 1.5.$$

With the magnetic field along the x-axis, this means that $p = (25 \pm 10)\%$ of the radiation is elliptically polarized with the major axis at $(90 \pm 10)^\circ$ to the x-axis, $E_x/E_y = (0.2 \pm 0.3)$ and the more probable sense is left-handed. The measurement uncertainties are consistent with plane polarization in the extraordinary mode and should be significantly reduced with an improved version of the polarimeter presently under construction.

THEORY

If the optical depth τ, for radiation in the resonant layer is such that $\tau \gg 1$ then the intensity of ECE corresponds to the black body level[7]. For the second harmonic under typical tokamak conditions $q = (\omega_{pe}/\omega)^2 \lesssim 1$. Hence instead of the very low density, ($q \ll 1$), theory[3] used to estimate

$\tau_{o,e}$ for the ordinary (o) and extraordinary (e) modes we use the general expression for the ℓth harmonic cyclotron damping in a plasma of finite density[8] and the usual slab model for the resonant layer[3]. Thus for the second harmonic:

$$\tau_{o,e} = 4\pi^2 \left(\frac{kT}{m_o c^2} \right) \frac{R}{\lambda} \; G(q,\theta) \cos \beta$$

where: R = major radius, λ = free space wavelength, T = electron temperature, θ is the angle between the wave vector and the magnetic field and β is the angle between the wave vector and the Poynting vector.

$$G(q,\theta) = 3q n^3 \sin^2 \theta \, \frac{[n^4 \sin^2 \theta - n^2(1-q)(1+\cos^2\theta) + 2(1-2q)(1-q-n^2\sin^2\theta)]}{2\,(1-2q)\,(3-2q)(1-q-n^2) - qn^2(1+\cos^2\theta)}$$

where $n = n_{o,e}(q,\theta)$ is the cold plasma refractive index. The neglect of relativistic line-broadening is valid for $n\cos\theta \gtrsim \sqrt{kT/mc^2}$, typically $\theta \lesssim 88^\circ$. Figure 3 shows a plot of $G(\theta)$ for $q = 0.1$ and 0.2 (for which $\cos\beta \simeq 1$) indicating that although $\tau_o \ll \tau_e$ for $\theta \simeq 90^\circ$, for $\theta \simeq 70^\circ$ $\tau_o \sim \tau_e$.

In the experiment the antenna receives radiation over angles $87^\circ < \theta \lesssim 90^\circ$. The angular variations of $\tau_{o,e}(\theta)$ are insufficient to explain the low degree of polarization observed unless a significant amount of black body radiation in the o-mode from $\theta \lesssim 70^\circ$ is refracted by the plasma into the antenna. Numerical computations of $\tau_{o,e}$ along refracted ray paths confirm that this effect can bring about substantially unpolarized emission at $\theta = \pi/2$, previously attributed to polarization scrambling by wall reflections[1].

REFERENCES

(1) A.E. Costley, R.J. Hastie, J.W.M. Paul and J. Chamberlain, Phys. Rev. Lett. 33 (1974) 758.
(2) F.J. Stauffer and D.A. Boyd, Infrared Physics, 18 (1978) 755.
(3) F. Englemann and M. Curatolo, Nuclear Fusion 13 (1973) 497.
(4) D.V. Bartlett, A.E. Costley and L.C. Robinson, Infrared Physics, 18 (1978) 749.
(5) A.E. Costley and TFR Group, Phys. Rev. Lett. 38 (1977) 1477.
(6) I.H. Hutchinson and D.S. Komm, Nuclear Fusion 17 (1977) 1077.
(7) V.I. Pakhomov, V.F. Aleksin and K.N. Stepanov, Sov. Phys. Tech. Phys. 6 (1962) 856.
(8) A.I. Akhiezer et al "Plasma Electrodynamics" Vol 1, Pergamon Press, (Oxford, 1975).

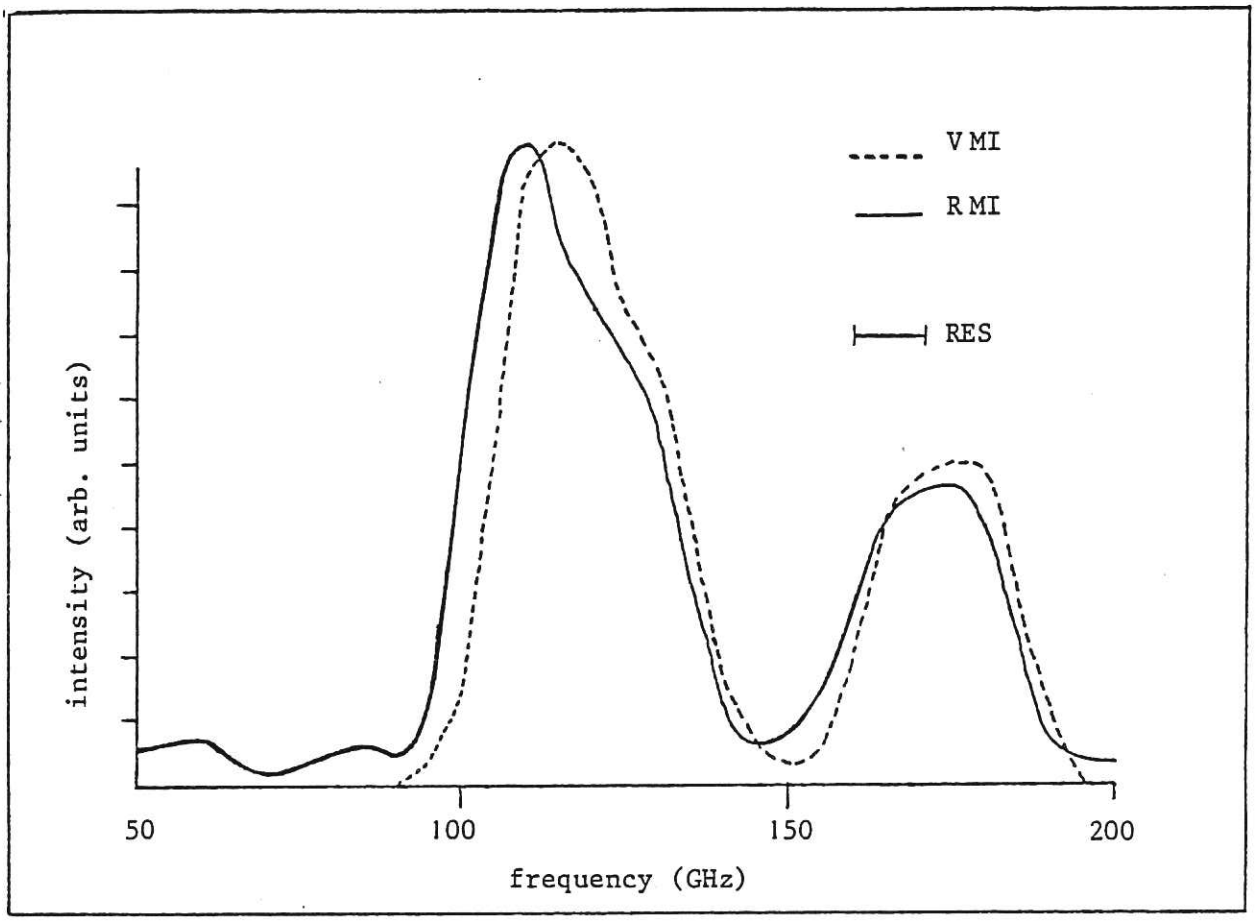

Fig. 1. Comparison between spectra from vibrating mirror interferometer (VMI) and rotating mirror interferometer (RMI). RES is the frequency resolution of both instruments.

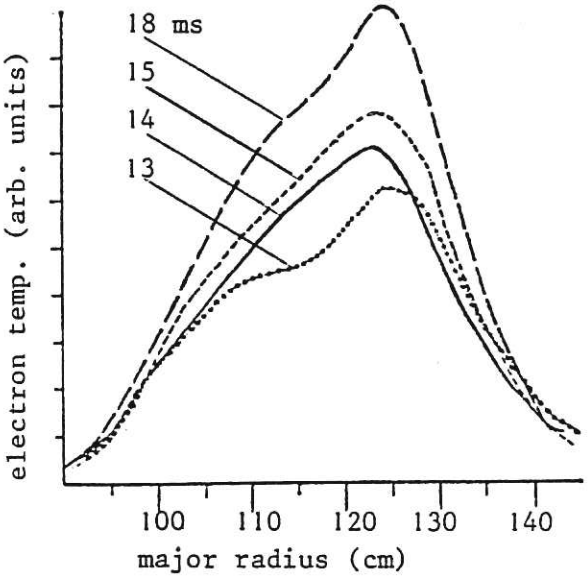

Fig. 2. Sequence of temperature profiles taken at early times during discharge.

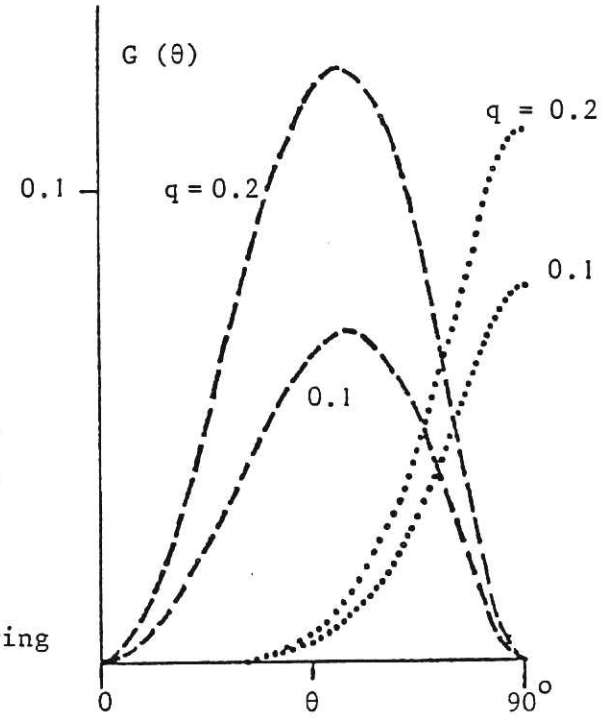

Fig. 3. The function G(θ) for q = 0.1 and q = 0.2. Dashed line o-mode, dotted line e-mode.

Errata: Paper EP 13 by Campbell et al

a) The measured Stokes parameters in the second section of the paper should be $I_o = 23 \pm 1$, $I_p = 4.5 \pm 1.5$, $M = -4 \pm 1$, $C = 0 \pm 1.5$, $S = -1.0 \pm 1.5$. The units are in units of intensity of an arbitrary value.

b) Due to a sign error in reference (8), the function $G(q,\theta)$, for the angular variation of the optical depth $\tau_{o,e}$, is incorrect. The correct form should be:

$$G(q,\theta) = 3q\,n^3 \sin^2\theta \, \frac{[n^4 \sin^2\theta - n^2(1-q)(1+\cos^2\theta) + 2(1-2/3\,q)\,(1-q-n^2\sin^2\theta)]}{2(1-2q)\,(3-2q)\,(1-q-n^2) - qn^2\,(1+\cos^2\theta)} .$$

As a consequence, in contrast to Fig. 3, the correct behaviour of $G(q,\theta)$ indicates that the optical depth for the O-mode at oblique angles is an order of magnitude smaller than the e-mode and the finite density theory gives a small correction to the result obtained from the low density theory given in reference (3). A particular result for $q = 0.2$ is shown in the figure below.

The absence of strong polarisation in the observed emission can thus be explained only by taking account of wall reflections as in reference (1).

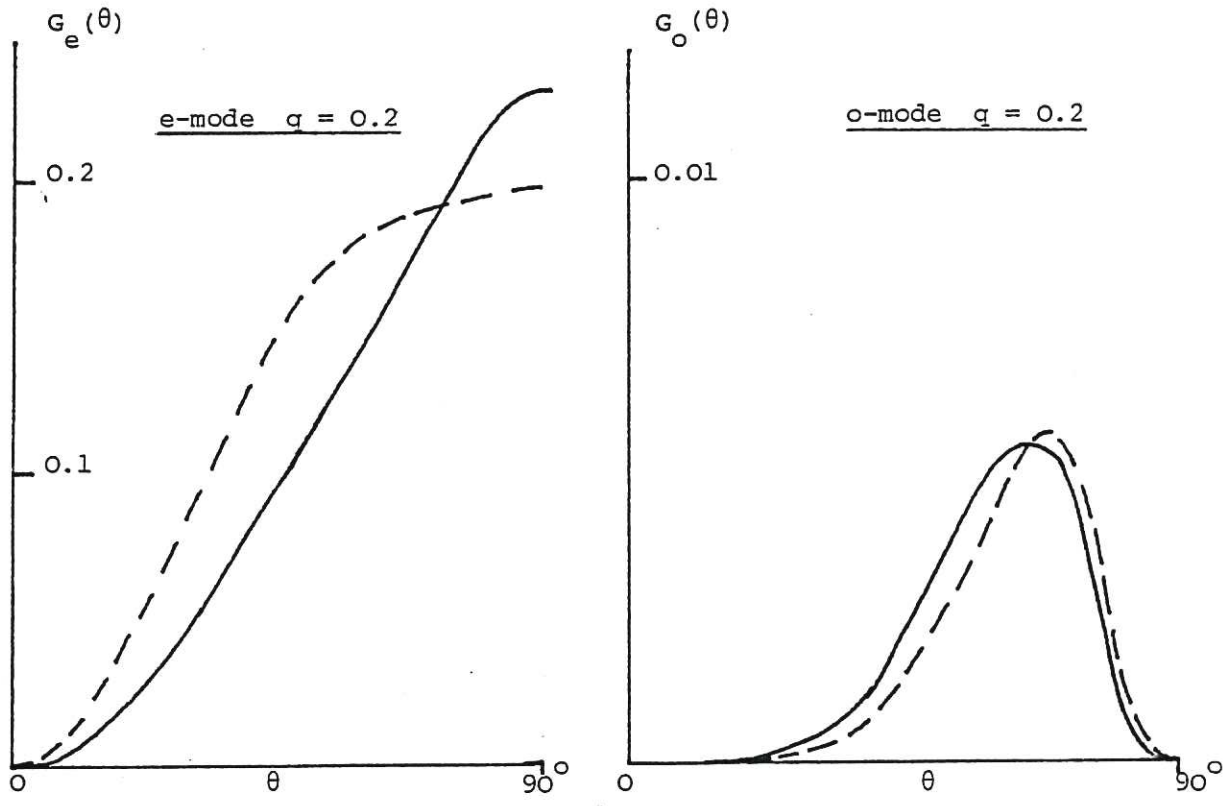

The function $G(q,\theta)$ for $q = 0.2$. Dashed line is the corresponding variation according to the low density theory of reference (3).

MEASUREMENTS OF ELECTRON CYCLOTRON EMISSION ON T-10

A.A. Bagdasarov*, W.H.M. Clark, A.E. Costley‡, E.P. Gorbunov* and G.F. Neill‡

Culham Laboratory, Abingdon, Oxon, OX14 3DB, UK
(Euratom/UKAEA Fusion Association)

* The I.V. Kurchatov Institute of Atomic Energy, Moscow, U.S.S.R.
‡ The National Physical Laboratory, Teddington, UK

ABSTRACT

Measurements of the electron cyclotron emission from the T-10 tokamak plasma are presented. From these the spatial profiles of the electron temperature are deduced and compared with measurements from Thomson scattering. In general there is good agreement but in some cases structure is observed on the profiles. It is possible that this is due to the presence of trapped electrons. Attempts to measure the emission during experiments on ECRH were unsuccessful because of interference, but we can conclude that ECRH does not leave the electron velocity distribution disturbed after the pulse.

EXPERIMENTAL ARRANGEMENT

In this paper we report results of a joint UK/USSR experiment on the T-10 tokamak where the primary objective was to measure the spectrum of electron cyclotron emission and to deduce the spatial profile of the electron temperature. Attempts were also made to measure the emission during electron cyclotron resonance heating (ECRH) experiments on the plasma.

Radiation emitted from the outside of the tokamak at 10^{o} to the equatorial plane was transmitted by over-moded waveguides (dia. > 10 x maximum wavlength) to a rapid-scan polarization type interferometer[1] fitted with a liquid helium cooled indium antimonide detector. The instrument measures the emission spectrum in the frequency range $50 < f < 500$ GHz, that is $f_{ce} < f < 6f_{ce}$ for toroidal flux density $B_T = 3.0$ T, where f_{ce} is the electron cyclotron frequency. The time resolution is ~ 14 ms and the spectral resolution $\gtrsim$ 7 GHz. A dedicated minicomputer system (SADA) is used to control the interferometer remotely, and to analyse, display and record the data in the time interval between shots (typically 10 mins). The interferometer was calibrated with single frequency microwave sources and with a black body source at liquid nitrogen temperature.

In addition, the emission around fixed frequencies was measured with a Fabry-Perot interferometer operating in first order with a resolving power $\gtrsim$ 20. A multi-element low pass filter is included in the device to prevent transmission of the higher orders. In principle, the time

resolution of this device is determined by the bandwidth of the detector ($\lesssim$ 300 kHz) but for the measurements reported here the radiation was amplitude modulated at 200 Hz to minimize effects due to pick-up.

Some preliminary measurements were also made with a scanning Fabry-Perot interferometer where one of the plates was vibrated at 100 Hz. With this device it is possible to measure the emission in narrow regions of the spectrum, e.g. $1.8\ f_{ce} < f < 2.2\ f_{ce}$, with a spectral resolving power $\sim$ 20 and a time resolution $\sim$ 5 ms.

RESULTS

Two types of plasma discharges were investigated. In type I, B_T = 3.0 T, plasma current $I_g \sim 400$ kA, typical line-average electron density $\bar{n}_e \sim 2 \times 10^{19}$ m^{-3} and electron temperature $T_e \sim 800$ eV. For type II, B_T = 1.5 T, $I_g \sim 200$ kA, $\bar{n}_e \sim 1.5 \times 10^{19}$ m^{-3} and $T_e \sim 1.2$ keV.

Under conditions I the emission spectra are usually of the form shown in Fig. 1. Since for these conditions the plasma is optically thick for most of the second harmonic (see Fig. 2) it should be possible to determine the spatial dependence of the electron temperature by using the usual frequency to space transformation[2]. An example is shown in Fig. 3 along with the corresponding Thomson scattering points. The profiles obtained at other times on the same shot are also shown. We note that the agreement is generally good but that the profile from cyclotron emission is slightly narrower. This is possibly due to a reduction in optical depth and therefore a departure from black-body conditions in the wings of the line.

One interesting feature is the apparent structure on the line which under some circumstances can be relatively large. The plasma emission results suggest that this may be real, although at present the signal-to-noise on the calibration is insufficient to be sure of the exact shape. In view of the high thermal conductivity along the magnetic surfaces it is unlikely that this represents real structure in the temperature profile. One possible explanation is emission by trapped electrons, i.e. localised suprathermals, and it is interesting to note that independent soft X-ray measurements have shown that such particles exist in T-10 particularly on the outside of the plasma (i.e. at major radii > 1.5 m)[3].

Under conditions II similar spectra are obtained but in this case the deduction of the electron temperature profile is less reliable because of cut-offs in the emission due to finite density effects[4]. Nevertheless, the profiles still seem to be in approximate agreement with Thomson

scattering, possibly because of the spatial averaging in the emission measurement arising from antenna pattern, frequency resolution and refraction effects.

With experiments on ECRH at the second harmonic extraordinary mode under type II conditions no measurements could be made during the heating pulse (peak power $\lesssim$ 250 kW, duration $\lesssim$ 50 ms) because of severe pick-up. However, measurements made immediately before and after the pulse showed little change in the spectrum, as shown in Fig. 4. No heating effect was observed but this is probably because the time delay for the system to recover from the pick-up was of the same order as the energy confinement time ($\sim$ 15 ms under these conditions). Nevertheless, it is possible to conclude that the heating does not produce distortions to the electron velocity distribution lasting longer than 15 ms. It will be necessary to use a system specifically designed for minimum sensitivity to radiative and electrical pick-up to obtain measurements during the heating pulse.

ACKNOWLEDGEMENTS

We wish to thank Drs Berlizov, Dnestrovskii, Notkin and Razumova for information and useful discussions, Dr B. Walker for supplying the Fabry-Perot interferometers and the T-10 tokamak group for their co-operation.

REFERENCES

(1) A.E. Costley and J. Chamberlain, Conf. on Precision Electromagnetic Measurements, IEE, No 113, 210 London (1974).
(2) F. Engelmann and M. Curatolo, Nuclear Fusion 13 (1973) 497.
(3) K.A. Razumova and D. Marty, Private communication.
(4) C.M. Celata and D.A. Boyd, Nuclear Fusion 19 (1979) 423.
(5) Yu. N. Dnestrovskii, D.P. Kostomarov and N.V. Skrydlov, Sov. Phys. Tech. Phys. 8 (1964) 691.

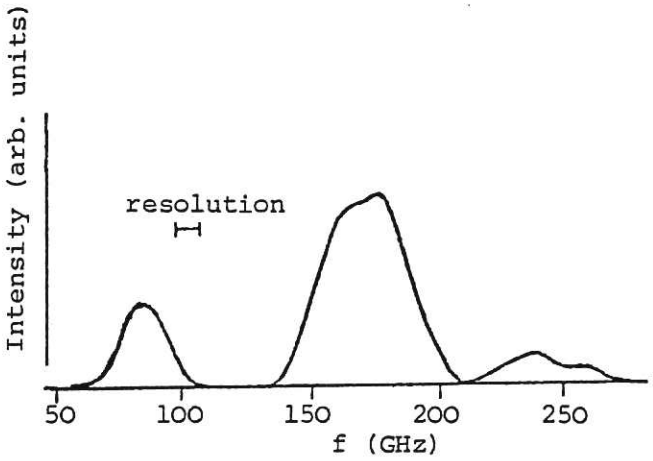

Fig. 1. Emission spectrum under type I conditions.

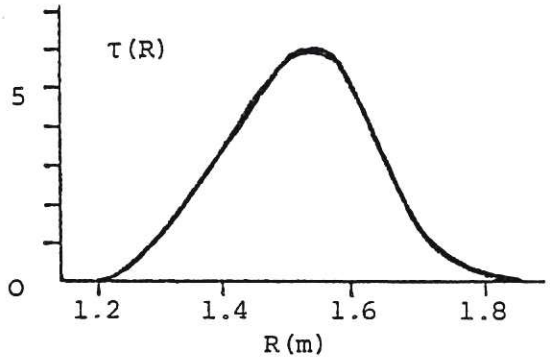

Fig. 2. Plasma optical depth τ as a function of major radius R calculated using expressions derived from Ref. (5) and probable density and temperature profiles. We note that it should be possible to determine $T_e(R)$ in the range $1.3 < R < 1.7$ m from emission measurements.

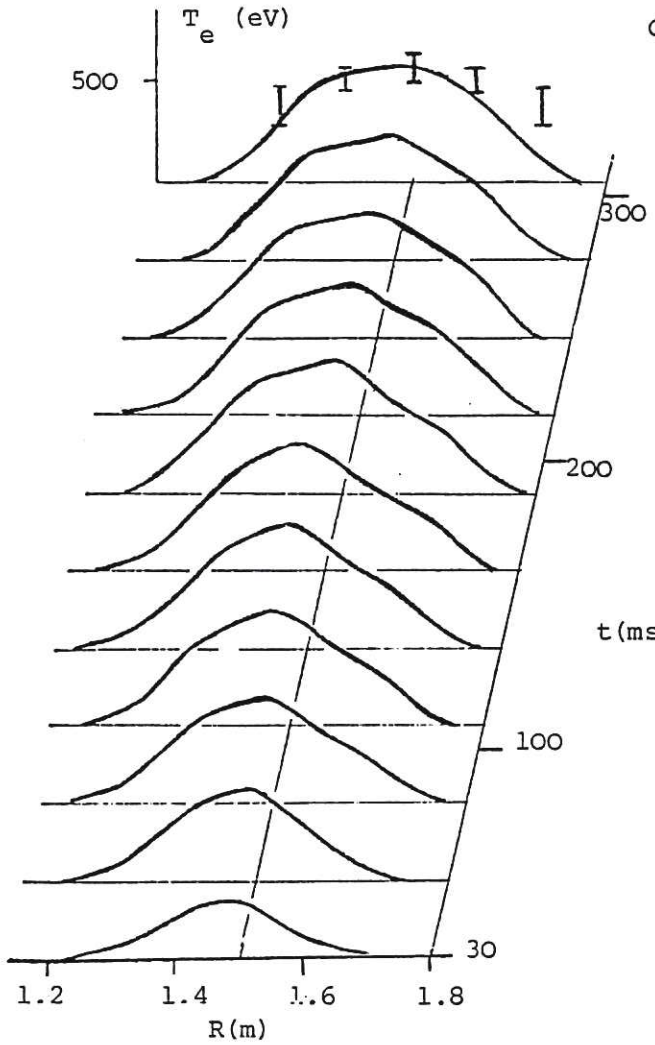

Fig. 3. $T_e(R,t)$ deduced from emission measurements and comparison with Thomson scattering. Emission profile is normalised to Thomson profile at R = 1.5 m.

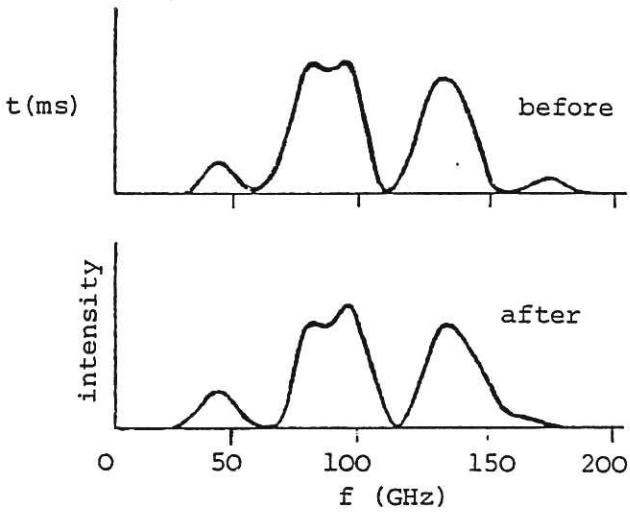

Fig. 4. Spectrum just before (~ 15 ms) and just after (~15 ms) the ECRH heating pulse (power ~ 120 kW, duration = 20 ms).

PELLET REFUELLING OF A DIVERTOR TOKAMAK

L.W. Jørgensen and P.E. Stott*

Culham Laboratory, Abingdon, Oxon, OX14 3DB, UK
(Euratom/UKAEA Fusion Association)

INTRODUCTION Experiments with the DITE Bundle Divertor have demonstrated the need for a new means of refuelling a diverted discharge in order to replace the particles exhausted by the divertor and thus maintain a constant density[1]. Refuelling with gas puffed into the torus has been shown to be inefficient because a large fraction of the gas is ionised in the divertor scrape-off layer and immediately exhausted leaving only a small fraction to penetrate and refuel the centre of the discharge. Increasing the input of gas to counteract this loss results in increased recycling between the plasma boundary and the wall which in turn results in increased desorption of impurities.

Injection of solid hydrogen pellets has been proposed as a method of refuelling a future fusion reactor, and the technique has been demonstrated recently in an experimental tokamak[2]. A pellet with sufficiently high velocity will penetrate the scrape-off layer with only a small loss of material and will refuel the centre of the discharge. A pellet acceleration device based on a light gas gun system is being constructed for DITE. Initially, the plan is just to accelerate a single cylindrical pellet with a diameter and length of about 400 μm to a velocity of about 400 m/s with the purpose of testing ablation models and studying the effect of injecting fresh fuel across the divertor scrape-off layer. SI-units are used throughout this paper except when stated otherwise. Temperatures are given in eV.

PELLET ABLATION RATE Many different models of pellet ablation in a hot plasma have been presented[3]. The most recent models assume that a neutral cloud of gas is established around the pellet[4,5] and the pellet ablation rate is determined by the maintenance of cloud thickness equal to the penetration depth of the plasma electrons. Comparing the different models for pellet-plasma interaction with the few available experimental results of pellet injection show[2,3,6,7] that in present day tokamaks the pellet-plasma interaction can be explained by this neutral cloud model.

The results of the different neutral cloud models have been compared[7] and it is concluded that the ablation rates which they predict have almost identical scaling. Hence we will use the following convenient "average" pellet ablation rate for a spherical pellet

$$\dot{r}_p = - f\, r_p^{-2/3}\, n_e^{1/3}\, T_e^{5/3} \qquad \ldots (1)$$

where r_p is the instant pellet radius; n_e and T_e are the plasma electron density and temperature; f is a material constant; $f_{H_2} = 8 \times 10^{-14}$; $f_{D_2} = 5.6 \times 10^{-14}$.

We will assume linear profiles for the plasma density $n_e = n_{eo}\,(1 - r/a)$ and temperature $T_e = T_{eo}\,(1 - r/a)$ where a is the minor radius of the torus. Inserting these profiles in Eq.(1) using $v_p t = a - r$, where v_p is the pellet velocity, gives

$$r_p = \left(r_{po}^{5/3} - \frac{5}{9} f \frac{a\, n_{eo}^{1/3}\, T_{eo}^{5/3}}{v_p} (1 - r/a)^3\right)^{3/5} \qquad \ldots (2)$$

and a pellet penetration depth of

$$d = \left(\frac{9}{5f}\right)^{1/3} a^{2/3}\, n_{eo}^{-1/9}\, T_{eo}^{-5/9}\, r_{po}^{5/9}\, v_p^{1/3} \qquad \ldots (3)$$

where r_{po} is the initial radius of the pellet.

---

* Present address: JET Joint Undertaking, Abingdon, Oxon, OX14 3EA.

For non-perpendicular (to the toroidal magnetic field) pellet injection the perpendicular component of the velocity vector is used in Eqs.(2) and (3). In order to derive an ablation equation as (1) it is necessary to assume[4,5] that the number of pellet atoms, N_p, is small compared to the total number of plasma ions, N, otherwise the presence of the pellet in the plasma will significantly change the plasma density and temperature, which in turn will change the ablation rate of the pellet.

Figure 1 shows the pellet penetration depth versus the pellet velocity for different plasma parameters. We have shown also the value of the ratio $N_p/N = 2n_s r_{po}^3/\pi a^2 R\, n_{eo}$, where n_s is the atomic density of solid hydrogen; R is the major radius of the torus. It is seen that these relatively slow pellets have penetration depths deeper than the scrape-off layer, but smaller than the distance to the centre of the plasma.

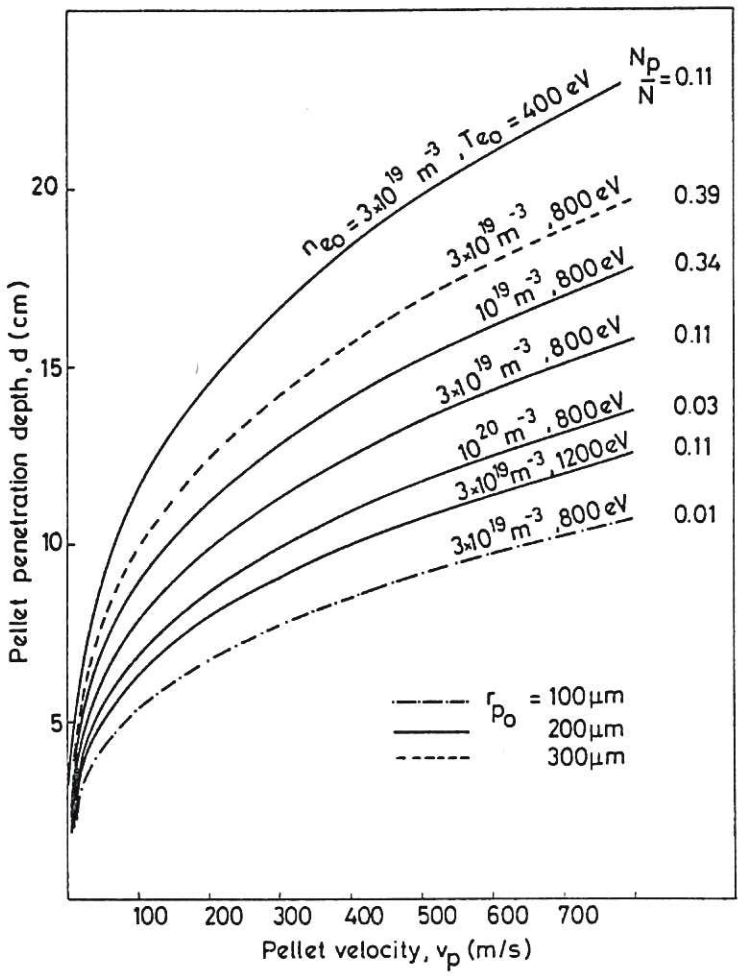

Fig. 1. Pellet penetration depth

DEPOSITION OF THE PELLET MATERIAL

Besides estimating the pellet penetration depth it is very important to see how the ablated material is deposited in relation to the plasma density profile.

The Ablating Pellet as a Point Source. In this section we assume the pellet to be a point source emitting atomic ions and electrons with a rate given by Eq.(1). Due to the magnetic field configuration, the amount of ablated hydrogen ions in a toroidal shell with radius r and thickness dr is $n_s 4\pi\, r_p^2 |\dot{r}_p| dt$, and as the parallel transport of ionised material is large we will assume these ions fill the toroidal shell uniformly, so that the density is:

$$n_p(r) = \frac{n_s\, 4\pi\, r_p^2 |\dot{r}_p| dt}{2\pi\, r\, dr\, 2\pi\, R} = \frac{f\, n_s}{\pi R\, r\, v_p}\, r_p^{4/3}\, n_e^{1/3}\, T_e^{5/3}. \qquad \ldots (4)$$

In Fig. 2 we show in the curves marked $\delta = 0$ the resulting plasma density profile for a typical set of parameters. It is seen that even for low values of N_p/N there will be rather high local plasma density perturbations; with peak values of $n_p/n_e \approx 3N_p/N$.

Ionisation Radius of the Ablation Cloud. In the previous section we assumed the pellet to be a point source of atomic ions and electrons but this is not entirely correct since the pellet-plasma model we use is based on the development of a neutral cloud of hydrogen molecules

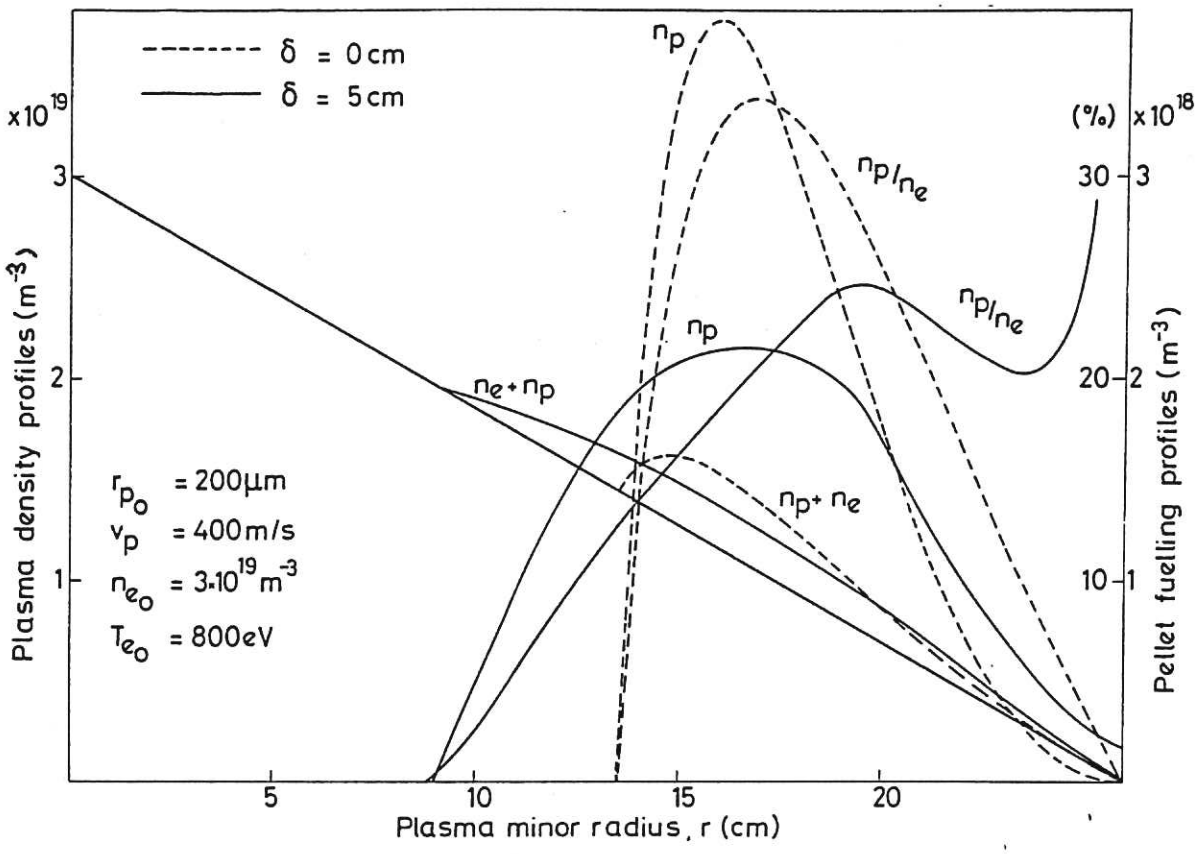

Fig. 2. Ablated pellet material profiles

around the pellet. This cloud is heated by the energetic plasma electrons which drive the molecules outwards until they reach the point where they are ionised. The dominant ionisation process is $H_2 + e \rightarrow H_2^+ + 2e$[8]. The point at which most of the molecules are ionised is defined as the "ionisation radius", r_I[5]. It is shown that: $r_I/r_p \gg 1$; r_I is almost independent of the values of r_p; and r_I decreases for increasing plasma density and increases for increasing plasma temperature.

After ionisation the H_2^+ ions are constrained to follow the magnetic field lines. The dominant process is then dissociation, $H_2^+ + e \rightarrow H^+ + H^o + e$. The mean free path length for this process is somewhat smaller than the value of r_I. Hence the overall picture is that the pellet material results in equal numbers of cold ions and neutral atoms smeared out over a region $(r - \delta, r + \delta)$ where $\delta \gtrsim r_I$. Assuming a uniform production rate of ions within this interval we have for $d > \delta$

$$n_p(r) = \frac{\int_{t1}^{t2} \frac{dr}{2\delta}\, n_s\, 4\pi\, r_p^2 |\dot{r}_p| dt}{2\pi r \;\; dr \;\; 2\pi R} \qquad \ldots (5)$$

where $t_1 = \begin{cases} 0 \text{ for } a - \delta \le r \le a \\ \frac{a - \delta - r}{v_p} \text{ for } r \le a - \delta \end{cases}$ $\qquad t_2 = \begin{cases} \frac{a + \delta - r}{v_p} \text{ for } a - d + \delta \le r \\ \frac{d}{v_p} \text{ for } r \le a - d - \delta. \end{cases}$

In order to carry out this integration we shall simply assume a constant value of δ which is reasonably well justified since the pellet travels towards both higher plasma density and temperature[5]. Hence from Eq.(5) we find

$$n_p(r) = -\frac{n_s}{6\pi R \delta r} [r_p^3]_{t1}^{t2} \qquad \ldots (6)$$

where r_p is given in Eq.(2). Figure 2 shows how the fuelling profile and resulting plasma density profile are changed when taking into account a finite radius of the ablation cloud. The fuel is spread out and a larger fraction of the fuel is deposited deeper in the plasma. This also results in a smaller local plasma perturbation, $n_p/n_{e|max} \sim 2\, N_p/N$.

TRANSPORT OF NEUTRAL PELLET ATOMS. In this section we deal with the transport of the neutrals which originate from the ablating pellet. We include these neutrals as a source term, $S_n(r)$ in a steady-state recycling code for neutral plasma particles. The cold neutrals from the pellet charge-exchange with hot plasma ions and the resulting hot neutrals are able to penetrate deep into the plasma. Because the charge-exchange cross-section is several times larger than the ionisation cross-section, several generations of hot neutrals are possible before the final ionising collision occurs. The steady-state approximation is valid in cases where the pellet repetition time, (Δt) is only a few times larger than the pellet ablation time so that we can assume $S_n(r) \simeq \frac{1}{2} n_p(r)/\Delta t$, where $n_p(r)$ is given from Eq.(6). This expression will, of course, be better fulfilled for several pellet launchers distributed around the torus. Figure 3 shows the results of the calculations for the same case as in Fig. 2.

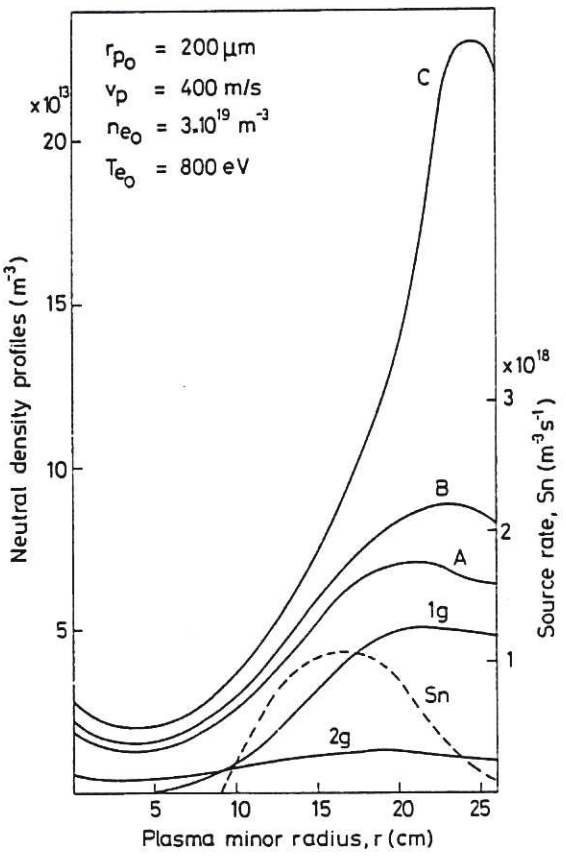

Fig. 3. Neutral density profiles calculated for a pellet injection rate normalised to one pellet per second. Values for an injection rate of η pellets per second can be obtained by multiplying these results by a factor η. The curve S_n shows the source rate of cold neutrals (energy 10 eV) from the ablating pellet. The curves 1g and 2g show the first and second generations of more energetic neutrals produced by charge-exchange. Three boundary conditions are compared: (A) a non-reflecting wall which traps all incident neutrals; (B) a partly-reflecting wall from which neutrals are reflected with reduced energy and with an energy dependent reflection coefficient; (C) a partly reflecting wall as (B) plus gas desorption. A cold (10 eV) neutral is released to replace every incident neutral which is trapped on the wall.

CONCLUSIONS. It is shown that relatively slow pellets (about 300 - 600 m/s) penetrate beyond the divertor scrape-off layer but do not reach the centre of the plasma. However, if the finite size of the pellet ablation cloud is taken into account, a large fraction of the fuel is deposited much deeper in the plasma and there is less local plasma density perturbation. Half of the ablated pellet ends up as neutral atoms and steady-state transport calculations show that these atoms penetrate even deeper into the plasma resulting in a significant neutral density at the centre of the plasma.

REFERENCES

(1) S.J. Fielding et al, 8th Europ. Conf. on Controlled Fusion, Prague (1977) 1, 36.
(2) S.L. Milora et al, Phys. Rev. Letts. 42 (1979) 97.
(3) Proc. Fusion Fuelling Wksp. (Princeton) U.S. Dept. of Commerce, CONF-771129 (1978).
(4) D.F. Vaslow, IEEE Transaction on Plasma Science, 5 (1977) 12.
(5) P.B. Parks et al, Nuclear Fusion 17 (1977) 539.
(6) C.A. Foster et al, Nuclear Fusion 17 (1977) 1067.
(7) L.W. Jørgensen and A.H. Sillesen, Ablation of Solid Hydrogen in a Plasma, Submitted for publication in J. Phys. D.
(8) R.L. Freeman and E.M. Jones, Atomic Collision Processes in Plasma Physics Experiments I + II, CLM-R 137 (1974) and CLM-R 175 (1977).
(9) G.M. McCracken and P.E. Stott, Nuclear Fusion (to be published), CLM-P573.